



# Lawrence Berkeley Laboratory

UNIVERSITY OF CALIFORNIA

## Materials & Chemical Sciences Division

Submitted to the Journal of the American Ceramic Society

### Rare-Earth Disilicate-Silicon Nitride Ceramics: II. Oxidation Behavior

M.K. Cinibulk, G. Thomas, and S.M. Johnson

November 1991



1 LOAN COPY 1  
1 Circulates 1  
1 for 4 weeks 1 Bldg. 50 Library.  
Copy 2

LBL-31454

#### DISCLAIMER

This document was prepared as an account of work sponsored by the United States Government. Neither the United States Government nor any agency thereof, nor The Regents of the University of California, nor any of their employees, makes any warranty, express or implied, or assumes any legal liability or responsibility for the accuracy, completeness, or usefulness of any information, apparatus, product, or process disclosed, or represents that its use would not infringe privately owned rights. Reference herein to any specific commercial product, process, or service by its trade name, trademark, manufacturer, or otherwise, does not necessarily constitute or imply its endorsement, recommendation, or favoring by the United States Government or any agency thereof, or The Regents of the University of California. The views and opinions of authors expressed herein do not necessarily state or reflect those of the United States Government or any agency thereof or The Regents of the University of California and shall not be used for advertising or product endorsement purposes.

Lawrence Berkeley Laboratory is an equal opportunity employer.

## **DISCLAIMER**

This document was prepared as an account of work sponsored by the United States Government. While this document is believed to contain correct information, neither the United States Government nor any agency thereof, nor the Regents of the University of California, nor any of their employees, makes any warranty, express or implied, or assumes any legal responsibility for the accuracy, completeness, or usefulness of any information, apparatus, product, or process disclosed, or represents that its use would not infringe privately owned rights. Reference herein to any specific commercial product, process, or service by its trade name, trademark, manufacturer, or otherwise, does not necessarily constitute or imply its endorsement, recommendation, or favoring by the United States Government or any agency thereof, or the Regents of the University of California. The views and opinions of authors expressed herein do not necessarily state or reflect those of the United States Government or any agency thereof or the Regents of the University of California.

**Rare-Earth Disilicate–Silicon Nitride Ceramics:  
II. Oxidation Behavior**

Michael K. Cinibulk<sup>\*\*</sup> and Gareth Thomas<sup>#</sup>

Department of Materials Science and Mineral Engineering  
University of California  
and  
Center for Advanced Materials  
Materials Sciences Division  
Lawrence Berkeley Laboratory  
University of California  
Berkeley, California 94720

Sylvia M. Johnson<sup>#</sup>

Materials Research Laboratory  
SRI International  
Menlo Park, CA 94025

November 1991

<sup>#</sup>Member, American Ceramic Society

<sup>\*</sup>Currently with Max-Planck-Institut für Metallforschung, Stuttgart, FRG

This work was supported in part by the National Science Foundation under Contract No. DMR 83-1317239 and by the Director, Office of Energy Research, Office of Basic Energy Sciences, Materials Sciences Division, of the U.S. Department of Energy under Contract No. DE-AC03-76SF00098.

## Abstract

The oxidation behavior and microstructure of the oxidized surfaces of  $\text{RE}_2\text{Si}_2\text{O}_7\text{-Si}_3\text{N}_4$  ceramics were investigated. The high oxidation resistance of these materials at  $1400^\circ\text{C}$  is attributed to the minimization of amorphous phases via devitrification to disilicates that are in equilibrium with  $\text{SiO}_2$ , the oxidation product of  $\text{Si}_3\text{N}_4$ . Crystals of  $\text{RE}_2\text{Si}_2\text{O}_7$  grew out of the surface silicate in preferred orientations that were dictated by crystal structure. The morphology of the microstructure of the oxidized surfaces was shown to be partially dependent on the concentration of impurities; the presence of Ca was found to coincide with the growth of  $\text{Gd}_2\text{Si}_2\text{O}_7$  and  $\text{Dy}_2\text{Si}_2\text{O}_7$  crystals with high aspect ratios. [Key Words: intergranular phase, microstructure, oxidation, rare-earth oxides, silicon nitride.]

## I. Introduction

Silicon nitride ceramics are among the most promising materials for use as structural components in high-temperature oxidizing environments. However,  $\text{Si}_3\text{N}_4$  is difficult to sinter to theoretical density without the use of additives that form a eutectic liquid through which mass transport, and hence densification, is enhanced. It is this liquid that forms the intergranular phase in  $\text{Si}_3\text{N}_4$  ceramics, on which the high-temperature behavior depends. Few studies have discussed the oxidation behavior of  $\text{Si}_3\text{N}_4$  sintered with oxides of the lanthanide metals.<sup>1-4</sup> In these investigations  $\text{Si}_3\text{N}_4$  sintered with only the lighter, less refractory lanthanides (La, Ce, and Sm) was studied. The oxidation resistance of  $\text{Y}_2\text{O}_3$ -sintered  $\text{Si}_3\text{N}_4$  has been found to be superior to that of the other  $\text{RE}_2\text{O}_3$ -sintered  $\text{Si}_3\text{N}_4$  materials.<sup>4</sup>

The design, fabrication, and microstructural characterization of  $\text{RE}_2\text{O}_3$ -sintered  $\text{Si}_3\text{N}_4$  ceramics tailored specifically for high temperatures has been previously described.<sup>5</sup> Lange et al.<sup>6</sup> have shown that in the  $\text{Si}_3\text{N}_4\text{-SiO}_2\text{-Y}_2\text{O}_3$  system,  $\text{Y}_2\text{Si}_2\text{O}_7$  is the most

oxidation resistant secondary phase for  $\text{Si}_3\text{N}_4$  ceramics because it is the only Y-containing phase in equilibrium with  $\text{SiO}_2$ , the oxidation product of  $\text{Si}_3\text{N}_4$ . The disilicates of the lanthanides should also be stable toward oxidation since phase relations in the  $\text{Si}_3\text{N}_4$ - $\text{SiO}_2$ - $\text{RE}_2\text{O}_3$  systems are generally considered to be analogous to those in the  $\text{Si}_3\text{N}_4$ - $\text{SiO}_2$ - $\text{Y}_2\text{O}_3$  system.<sup>7-9</sup> The crystallization behavior of all six disilicates as the secondary phases was similar, characterized by a limited nucleation and rapid growth mechanism resulting in large single crystals. Complete crystallization of the intergranular phase was obtained with the exception of a thin residual amorphous film which was observed at interfaces and believed to be rich in impurities, the cause of incomplete devitrification. In this paper the oxidation behavior and the microstructure of the oxidized surfaces of these  $\text{RE}_2\text{Si}_2\text{O}_7$ - $\text{Si}_3\text{N}_4$  materials is discussed.

## II. Experimental Procedure

### (1) *Material*

The sintered  $\text{Si}_3\text{N}_4$ <sup>†</sup> ceramics were prepared with a 2:1 molar ratio of  $\text{SiO}_2$ : $\text{RE}_2\text{O}_3$  (taking into account oxide present on the surface of  $\text{Si}_3\text{N}_4$  particles), placing the composition directly on the  $\text{Si}_3\text{N}_4$ - $\text{RE}_2\text{Si}_2\text{O}_7$  tie line.<sup>5</sup> These materials contain a 12.3 vol% grain-boundary phase; this volume fraction is equivalent to a 15 wt%  $\text{Y}_2\text{Si}_2\text{O}_7$ - $\text{Si}_3\text{N}_4$  material, which was found to sinter to >99 % theoretical density. The materials were subjected to a heat-treatment at 1400°C for 24 hr to crystallize the secondary  $\text{RE}_2\text{Si}_2\text{O}_7$  phase. X-ray diffraction and electron microscopy confirmed a completely crystalline secondary phase with a thin (1-10 nm) residual amorphous film at all two-grain boundaries for all materials with the exception of the  $\text{Yb}_2\text{Si}_2\text{O}_7$ - $\text{Si}_3\text{N}_4$  material. The  $\text{Yb}_2\text{Si}_2\text{O}_7$ - $\text{Si}_3\text{N}_4$  material had isolated regions with incompletely devitrified multiple-grain junctions, which were attributable to compositional heterogeneities in the powder compact during processing.

## (2) Oxidation

Oxidation studies were conducted at 1400°C over a period of ~200 hr in laboratory air. Samples 3 mm x 4 mm x 45 mm were cut from the sintered blocks. The surfaces were ground with a 320 grit diamond wheel, then polished to a 15 μm finish. Prior to oxidation, the surfaces were ultrasonically cleaned in acetone followed by a cleaning in ethanol. The specimens, on platinum wire supports in an alumina tray, were placed in a high-temperature box furnace at 400°C and heated to 1400°C within 15 min. The furnace was cooled to 400°C and the specimens removed at 12-48 hr intervals for weighing on an analytical balance having microgram resolution to determine weight change as a function of time. The materials were characterized by x-ray diffraction to identify crystalline phases present on the surfaces of the oxidized ceramics, which were scanned using Cu Kα radiation. The oxidized surfaces then were characterized by scanning electron microscopy and energy-dispersive x-ray spectroscopy.

## III. Results

### (1) Oxidation Kinetics

Fig. 1 is a plot of weight gain per unit surface area as a function of time at 1400°C. All materials had specific weight gains on the order of 0.25-0.35 mg/cm<sup>2</sup> after 192 hr with the exception of the Sm<sub>2</sub>Si<sub>2</sub>O<sub>7</sub>-Si<sub>3</sub>N<sub>4</sub> material which had a weight gain of 0.64 mg/cm<sup>2</sup> after the same time at temperature. The oxidation of sintered silicon nitride has been shown to obey a parabolic-type of rate law such that

$$W^2 = kt$$

where  $W$  is the weight gain per unit surface area,  $k$  is the parabolic oxidation rate constant, and  $t$  is exposure time.<sup>10</sup> Plotting these data parabolically results in straight lines for all curves but those for the Sm<sub>2</sub>Si<sub>2</sub>O<sub>7</sub>-Si<sub>3</sub>N<sub>4</sub> and Dy<sub>2</sub>Si<sub>2</sub>O<sub>7</sub>-Si<sub>3</sub>N<sub>4</sub> materials, as shown in

Fig. 2. The  $\text{Dy}_2\text{Si}_2\text{O}_7\text{-Si}_3\text{N}_4$  material deviates only slightly while  $\text{Sm}_2\text{Si}_2\text{O}_7\text{-Si}_3\text{N}_4$  departs significantly from linearity when plotted parabolically. The oxidation resistance of these materials can be correlated reasonably well with the refractoriness of the  $\text{RE}_2\text{O}_3\text{-SiO}_2$  system, i.e. inversely related to the eutectic temperature in each system. These temperatures are listed in Table 1. The  $\text{Y}_2\text{Si}_2\text{O}_7\text{-Si}_3\text{N}_4$  material fell in the middle of the group with respect to oxidation resistance while the  $\text{Er}_2\text{Si}_2\text{O}_7\text{-Si}_3\text{N}_4$  material displayed the best resistance toward oxidation.

Table I contains the parabolic oxidation rate constants for the six compositions investigated, as well as the total specific weight gain after 192 hr. The parabolic oxidation behavior of these ceramics indicates a diffusional process as the rate-limiting step in the oxidation mechanism, associated with the migration of additive ( $\text{RE}^{3+}$ ) and impurity cations along residual amorphous grain-boundary phases to the interface between ceramic and the surface oxide. The high oxidation resistance of these materials can be attributed to the presence of a minimal amount of amorphous grain-boundary phase, but with high viscosity due to the presence of refractory  $\text{RE}^{3+}$ , and the presence of thermodynamically stable crystalline secondary phases, such that the driving force for additive cation diffusion to the surface is minimized.

## (2) *Microstructure of Oxidized Surfaces*

The phases identified by x-ray diffraction composing the oxidized surfaces of the six materials are summarized in Table 3. X-ray diffraction patterns of the oxidized surfaces identified  $\alpha$ -cristobalite and the rare-earth disilicates to be the only major crystalline phases present. The disilicates crystallized on the surfaces into the same polymorphs as originally present as the secondary phase.<sup>5</sup> Also present were trace amounts of  $\beta\text{-Si}_3\text{N}_4$  and  $\text{Si}_2\text{ON}_2$ . The  $\beta\text{-Si}_3\text{N}_4$  peaks were smallest for those materials having the thickest oxide layers, indicating those signals were from the bulk ceramic beneath the oxidized surface layer. Spalling of the oxide from the substrate surfaces was not observed for any material.

SEM observations revealed the presence of two distinct morphologies for the rare-earth disilicates, a needle-like and a more equiaxed type. The oxidized surfaces also contained an amorphous silicate phase, from which cristobalite and  $\text{RE}_2\text{Si}_2\text{O}_7$  grains crystallized as shown in Figs. 3 and 4. Fig. 4 was obtained using backscattered electrons to gain contrast differences, strongly dependent on composition. In each image the darkest phase in the background is cristobalite, the intermediate phase surrounding the cristobalite grains is the residual amorphous silicate phase, and the phase in brightest contrast growing out of the silicate phase is the rare-earth disilicate. The dark jagged lines traversing the surfaces are cracks associated with either differential thermal expansion between the bulk and oxide layers or with the volumetric change accompanying transformation of surface cristobalite from the  $\beta$ - to  $\alpha$ -phase upon cooling.

The  $\text{Y}_2\text{Si}_2\text{O}_7$  crystals appear to have grown much larger in size than any of the other rare-earth disilicates and in a flattened elongated morphology. The x-ray diffraction patterns of the six materials indicated the disilicates crystallized in preferred orientations, with the  $[0\ 0\ 1]$  direction normal to the surface for those disilicates with tetragonal ( $A$ -phase) and orthorhombic ( $\delta$ -phase) crystal structures, and the  $[0\ 1\ 1]$  direction normal to the surface for those disilicates with monoclinic ( $\beta$ -phase) and triclinic ( $\alpha$ -phase) structures. A similar behavior of growth of  $\text{Y}_2\text{Si}_2\text{O}_7$  during oxidation has been reported by Babini et al.<sup>11</sup> with growth along the  $(1\ 1\ 0)$  plane and aligned parallel to the oxide surface. They found texturing of the  $\text{Y}_2\text{Si}_2\text{O}_7$  crystals to increase with temperature.

While the oxidized surface of the  $\text{Y}_2\text{Si}_2\text{O}_7$ - $\text{Si}_3\text{N}_4$  ceramic consisted exclusively of flattened and elongated  $\beta$ - $\text{Y}_2\text{Si}_2\text{O}_7$  crystals, the oxidized surfaces of the  $\text{Sm}_2\text{Si}_2\text{O}_7$ - $\text{Si}_3\text{N}_4$ ,  $\text{Er}_2\text{Si}_2\text{O}_7$ - $\text{Si}_3\text{N}_4$ , and  $\text{Yb}_2\text{Si}_2\text{O}_7$ - $\text{Si}_3\text{N}_4$  ceramics consisted exclusively of the respective disilicates in the equiaxed morphology. The oxidized surfaces of both the  $\text{Gd}_2\text{Si}_2\text{O}_7$ - $\text{Si}_3\text{N}_4$  and  $\text{Dy}_2\text{Si}_2\text{O}_7$ - $\text{Si}_3\text{N}_4$  ceramics contained disilicates of a needle-like morphology, but the equiaxed form still predominated. Because the needle-like morphology was observed only for disilicates having the orthorhombic structure, this

growth may be dependent on crystal structure. Energy dispersive x-ray spectroscopy of the disilicates indicated the presence of ~6-8 at.% Ca (as an impurity) associated with crystals having a whisker morphology while no appreciable Ca was detected in the equiaxed crystals. The cristobalite grains were found to be essentially free of impurities with less than 0.5 at.% Ca detected in the grains of all the materials. The remaining amorphous silicate phase surrounding the cristobalite grains had very high concentrations of impurity elements (~3-6 at.% each of Mg, Al, and Ca); these impurities are believed to have segregated to the grain-boundary phase from the  $\text{Si}_3\text{N}_4$  and  $\text{SiO}_2$  powders during sintering and then migrated to the surface during oxidation. Interestingly, this silicate phase was free from any but a trace amount of Fe.

#### IV. Discussion

##### (1) *Oxidation Mechanism and Kinetics*

The parabolic oxidation kinetics exhibited by sintered silicon nitride ceramics were originally assumed to be the result of a protective surface layer of  $\text{SiO}_2$ , as in the case of pure  $\text{Si}_3\text{N}_4$ . However, high-temperature exposure of silicon nitride sintered with oxide additives leads to accelerated oxidation attributable to the enhanced oxidation of  $\text{Si}_3\text{N}_4$  dissolved in a highly viscous silicate phase present at the surface.<sup>10</sup> The work of Singhal<sup>10</sup> and Cubicciotti et al.<sup>12,13</sup> showed that the outward diffusion of additive cations ( $\text{Mg}^{2+}$  or  $\text{Y}^{3+}$ , as well as impurities of  $\text{Al}^{3+}$ ,  $\text{Ca}^{2+}$ , and  $\text{Fe}^{3+}$ ) and nitrogen, produced by the amorphous intergranular-phase/oxide-layer diffusion couple, and the inward diffusion of oxygen resulted in a compositional gradient beneath the oxide layer. Therefore, the parabolic oxidation kinetics exhibited by sintered  $\text{Si}_3\text{N}_4$  ceramics is produced, not by a protective surface oxide layer, but by a compositional gradient lying beneath the oxidized surface layer.

The processed microstructures of these materials contained a thin residual amorphous film at all grain boundaries. Also, incomplete crystallization of the multi-grain junctions was observed in an isolated region of the  $\text{Yb}_2\text{Si}_2\text{O}_7\text{-Si}_3\text{N}_4$  material prepared for

transmission electron microscopy. The presence of residual amorphous grain-boundary phases, which are never in equilibrium with  $\text{SiO}_2$  (the oxidation product of  $\text{Si}_3\text{N}_4$ ), result in the creation of a driving force for additive and impurity cation diffusion to the  $\text{Si}_3\text{N}_4$ -bulk/oxide-layer interface. Impurities such as Mg, Al, Ca, and Fe are known to segregate to the amorphous intergranular phase during liquid-phase sintering. The presence of these impurities in addition to the additive cations ( $\text{RE}^{3+}$ ) determine to a great extent the properties of the amorphous phase.

In the materials studied, the secondary phases obtained are stable toward oxidation, therefore, the oxidation behavior was dependent solely on the amorphous intergranular-phase composition and the diffusion of its components to the bulk/oxide interface. The impurity content of the oxidized surfaces of all six materials was very similar, implying the differences obtained in oxidation behavior can be attributed to the effect of the additive cation ( $\text{RE}^{3+}$ ) on amorphous-phase viscosity. The oxidation resistance of these materials is related to the eutectic temperatures of the respective  $\text{RE}_2\text{O}_3$ - $\text{SiO}_2$  binary systems; i.e., in the binary systems with the highest eutectic temperatures, the materials sintered with these additives generally have shown the lowest weight gains. For these chemically similar grain-boundary phases, the viscosities are, therefore, assumed to be related to the eutectic temperatures. Although the amorphous phase contains N (which is estimated to lower the eutectic temperature of the  $\text{Y}_2\text{O}_3$ - $\text{SiO}_2$  system by  $\sim 140^\circ\text{C}$ , however raise its viscosity<sup>14</sup>), as well as the impurities mentioned, the effect of these constituents should be similar for all materials based on their similar compositions.

The one material which displayed greatly differing oxidation behavior was the  $\text{Sm}_2\text{Si}_2\text{O}_7$ - $\text{Si}_3\text{N}_4$  material. Whereas all other materials displayed, for the most part, parabolic oxidation kinetics, the  $\text{Sm}_2\text{Si}_2\text{O}_7$ - $\text{Si}_3\text{N}_4$  material deviated from this behavior and exhibited twice the weight gain as the other materials after 192 hr. Mieskowski and Sanders<sup>4</sup> also reported nearly twice the weight gain of a  $\text{Sm}_2\text{O}_3$ -sintered  $\text{Si}_3\text{N}_4$  material as that of a  $\text{Y}_2\text{O}_3$ -sintered  $\text{Si}_3\text{N}_4$  after 200 hr at  $1370^\circ\text{C}$ , however, they also reported parabolic

oxidation kinetics for both materials. Both materials were characterized as having completely amorphous grain-boundary phases.

The rate of weight gain of the  $\text{Sm}_2\text{Si}_2\text{O}_7\text{-Si}_3\text{N}_4$  material in the present study was very high at first and then decreased to a rate similar to that of the other five materials. The apparent departure of the oxidation behavior from that of parabolic may involve a reduction in surface area as oxidation progresses by the sealing of open porosity by the oxidation product, with the net effect being a steady increase in specific weight (assuming a constant surface area). The  $\text{Sm}_2\text{Si}_2\text{O}_7\text{-Si}_3\text{N}_4$  material had the lowest density (98%) of the six materials and therefore the existence of open porosity was likely. The increased surface area provided by porosity open to the surface initially would produce artificially high oxidation rates when calculating a surface area based on specimen dimensions alone. As oxidation proceeded and the pores were closed by oxidation product, this additional surface where reaction initially occurred would no longer be a source of reactant and the measured specific weight gain would approach the true weight gain per unit surface area as given by specimen geometry. Hence, following an initial period of oxidation where available surface area is continuously decreasing, the surface area becomes constant and parabolic oxidation kinetics are observed (Fig. 2).

The much higher apparent diffusivity of Sm cations through the grain-boundary phase than that of the other rare-earth cations cannot be explained on the basis of differences in eutectic temperatures of the systems alone. Although, the high specific weight gains initially occurring may be due to inaccurate estimates of surface area due to the presence of porosity, an additional explanation for the high rate of oxidation throughout the test may reside in the fact that Sm can exist in both the divalent and trivalent states.<sup>15</sup> Cerium can also exist in more than just the trivalent oxidation state. In  $\text{CeO}_2$ -sintered  $\text{Si}_3\text{N}_4$  ceramics,  $\text{CeO}_2$  is known to reduce to  $\text{Ce}_2\text{O}_3$  during sintering under inert conditions according to the reaction<sup>1,16</sup>



The mechanism proposed<sup>17</sup> for the oxidation of CeO<sub>2</sub>-sintered Si<sub>3</sub>N<sub>4</sub> ceramics, involves the migration of Ce<sup>3+</sup> cations from the grain-boundary phase to the bulk/oxide interface and subsequent dissolution in the amorphous surface silicate phase up to the equilibrium saturation, with excess Ce<sup>3+</sup> being oxidized to Ce<sup>4+</sup> by oxygen dissolved in the silicate resulting in the exsolution of CeO<sub>2</sub> crystals. Si<sub>3</sub>N<sub>4</sub> then dissolves in the silicate phase and reacts with the dissolved oxygen forming SiO<sub>2</sub> and the evolution of N<sub>2</sub>.

A similar reduction/oxidation reaction is proposed for Sm in Sm<sub>2</sub>Si<sub>2</sub>O<sub>7</sub>-Si<sub>3</sub>N<sub>4</sub> ceramics. Although the trivalent state is the characteristic one for all lanthanides and they can all exist in the divalent state under unusual conditions, only Sm, Eu, and Yb have significant "normal" chemistry in the divalent state.<sup>15</sup> Atypical oxidation states are most prevalent for lanthanides when the ion can have empty, half-filled, or filled *f*-shells. Analogous to the reaction involving the reduction of CeO<sub>2</sub> to Ce<sub>2</sub>O<sub>3</sub>, samarium could exist as Sm<sup>2+</sup> after reduction by dissolved nitrogen in the residual amorphous grain-boundary phase, which is known to be an oxynitride glass. The diffusion rate of divalent Sm is expected to be much greater than that of trivalent Sm,<sup>15</sup> which would account for the much greater weight gain upon oxidation of this material as compared with the weight gain of the other five materials. Upon reaching the bulk/oxide interface Sm<sup>2+</sup> dissolves in the surface silicate phase and is subsequently oxidized to Sm<sup>3+</sup>, reacts with dissolved SiO<sub>2</sub>, and precipitates out of solution as Sm<sub>2</sub>Si<sub>2</sub>O<sub>7</sub>. A problem with this hypothesis is that Yb can also exist in the divalent state, and as the observed oxidation kinetics of the Yb<sub>2</sub>Si<sub>2</sub>O<sub>7</sub>-Si<sub>3</sub>N<sub>4</sub> material are similar to those of the other four materials, there is no reason to suspect the reduction of Yb<sup>3+</sup> to Yb<sup>2+</sup>.

## (2). *Morphology of Oxidized Surfaces*

During the oxidation of sintered Si<sub>3</sub>N<sub>4</sub> materials, the surface silica produced as the oxidation product of Si<sub>3</sub>N<sub>4</sub> is brought to chemical equilibrium with those intergranular

phases not already existing in equilibrium with  $\text{SiO}_2$  (amorphous phase and incompatible crystalline phases) by the outward diffusion of additive and impurity cations. The equilibrium condition changes as oxidation proceeds and the grain-boundary phase becomes depleted of these cations. Precipitation of crystalline  $\text{RE}_2\text{Si}_2\text{O}_7$  and  $\text{SiO}_2$  from the surface silicate melt maintains chemical equilibrium with the changing grain-boundary phase composition. The growth of crystals in preferred directions can be explained in terms of relative entropy changes as associated with growth.<sup>17</sup> A large  $\Delta S$  results in the growth of faceted crystals due to anisotropic growth rates. A small  $\Delta S$  results in the growth of isotropic crystals due to low growth-rate anisotropy. A large  $\Delta S$  is expected for the growth of most inorganic compounds from the vapor phase or dilute solutions, including silicates from melts whereas a small  $\Delta S$  accompanies the growth of most metals and  $\text{SiO}_2$  from melts.<sup>17</sup> Figs. 3 and 4 indicate the isotropic growth of  $\text{SiO}_2$  and the faceted growth of the disilicates as predicted by differences in changes in entropy of crystal growth.

Previous investigations<sup>4,11</sup> have reported the growth of  $\text{RE}_2\text{Si}_2\text{O}_7$  crystals on the surface of the oxidized samples to be primarily in the form of needles and platelets. Babini et al.<sup>11</sup> have studied the effects of relative amounts of impurities in  $\text{Y}_2\text{O}_3/\text{SiO}_2$ -sintered  $\text{Si}_3\text{N}_4$  on the evolution of the morphology of the oxidized surfaces. They concluded that viscosity of the surface silicate phase, ionic mobility and degree of oversaturation of the diffusing cations in the surface silicate were closely related to the rate of oxidation, and that the morphology of the  $\text{Y}_2\text{Si}_2\text{O}_7$  crystallized in the oxidized surface was dependent on oxidation temperature, quenching rate, and ratio of impurities to  $\text{Y}^{3+}$  in the surface silicate.

All materials in the present investigation were oxidized under the same conditions (1400°C for ~200 hr) and according to the results of x-ray microanalysis, impurity concentrations in the oxidized surface layers of all six materials were about the same. The surfaces of all materials with the exception of the  $\text{Y}_2\text{Si}_2\text{O}_7$ - $\text{Si}_3\text{N}_4$  material contained  $\text{RE}_2\text{Si}_2\text{O}_7$  crystals of equiaxed morphology, with that of  $\text{Y}_2\text{Si}_2\text{O}_7$  being elongated and

plate-like. Only the  $\text{Gd}_2\text{Si}_2\text{O}_7\text{-Si}_3\text{N}_4$  and  $\text{Dy}_2\text{Si}_2\text{O}_7\text{-Si}_3\text{N}_4$  materials contained disilicates of the needle-like morphology and in both cases the needles contained  $\sim 6$  at.% Ca, while the same disilicates in the equiaxed morphology did not. It is likely that Ca acts to catalyze the growth of these crystals along preferred planes to form high aspect ratios resulting from highly anisotropic growth rates. By sintering  $\text{Si}_3\text{N}_4$  with the addition of a small amount of a dopant such as CaO, highly elongated  $\beta\text{-Si}_3\text{N}_4$  grains have been known to be catalyzed,<sup>18</sup> resulting in a microstructure that exhibits improved fracture toughness. Such a mechanism may be responsible for the formation of the needle-like  $\delta\text{-Gd}_2\text{Si}_2\text{O}_7$  and  $\delta\text{-Dy}_2\text{Si}_2\text{O}_7$  grains in the presence of high Ca concentrations.

The needle-like morphology was only assumed by the disilicates which have orthorhombic crystal structures. The  $\beta\text{-Er}_2\text{Si}_2\text{O}_7$  and  $\beta\text{-Yb}_2\text{Si}_2\text{O}_7$  forming the equiaxed, granular-like crystals are monoclinic as is  $\text{Y}_2\text{Si}_2\text{O}_7$  forming the flattened elongated crystals. The polymorphs of  $\text{RE}_2\text{Si}_2\text{O}_7$  observed by others<sup>4,11</sup> to grow into needle-like crystals were not identified, however the oxidation temperatures of  $\sim 1300\text{-}1400^\circ\text{C}$  suggest that the same polymorphs identified in the present study should have been present. The tetragonal structure of  $\text{A-Sm}_2\text{Si}_2\text{O}_7$  resulted in highly faceted crystals, not unlike those of the orthorhombic  $\delta\text{-Gd}_2\text{Si}_2\text{O}_7$  and  $\delta\text{-Dy}_2\text{Si}_2\text{O}_7$ .

## V. Conclusions

(1) The resistance to oxidation of these materials was about an order of magnitude better than that of other sintered  $\text{Si}_3\text{N}_4$  reported in the literature. The high oxidation resistance is attributed to the minimization of amorphous phases via devitrification to disilicates that are compatible with  $\text{SiO}_2$ , the oxidation product of  $\text{Si}_3\text{N}_4$ .

(2) The relative rates of oxidation found to be roughly inversely related to eutectic temperature of the  $\text{SiO}_2\text{-RE}_2\text{O}_3$  system, indicating that a lower viscosity residual amorphous phase results in a higher rate of oxidation as the rate-limiting step is diffusion of additive and impurity cations through this amorphous phase to the oxidized surface. The

oxidation behavior displayed by these materials was parabolic, which is consistent with previous studies which indicated that parabolic kinetics prevail during the oxidation of  $\text{Si}_3\text{N}_4$  ceramics.

(3) The oxidation of  $\text{Sm}_2\text{Si}_2\text{O}_7\text{-Si}_3\text{N}_4$  and  $\text{Dy}_2\text{Si}_2\text{O}_7\text{-Si}_3\text{N}_4$  was not found to display parabolic oxidation kinetics until after a certain exposure time. It is believed that the initially higher specific weight gains were obtained due to the presence of open porosity that was eventually sealed, leading subsequently to oxidation kinetics that were parabolic. The much higher oxidation rate of  $\text{Sm}_2\text{Si}_2\text{O}_7\text{-Si}_3\text{N}_4$ , even after sealing of porosity, could be due to the divalent nature of Sm in certain reducing environments, which would lead to enhanced transport to the oxidized surface.

(4) During oxidation  $\text{RE}_2\text{Si}_2\text{O}_7$  grew out of the surface silicate in preferred orientations that were dictated by crystal structure. The morphology of the microstructure of the oxidized surfaces was shown to be partially dependent on the concentration of impurities; the presence of Ca was found to coincide with the preferred growth of  $\text{Gd}_2\text{Si}_2\text{O}_7$  and  $\text{Dy}_2\text{Si}_2\text{O}_7$  into needle-like whiskers.

† SN E-10, Ube Industries, Tokyo, Japan

Based on the dissertation submitted by M.K. Cinibulk for the Ph.D. degree in Materials Science and Engineering, University of California, Berkeley, CA 94720

Presented in part at the 93rd Annual Meeting of the American Ceramic Society, Cincinnati, OH, April 30, 1991 (Symposium Paper No. 25-SII-91).

Initially supported by the National Science Foundation under Contract No. DMR 83-1317239. Additional support was provided by the Director, Office of Energy Research, Office of Basic Energy Sciences, Materials Sciences Division of the U.S. Department of

Energy under Contract No. DE-AC03-76SF00098. Additional facilities were provided by SRI International.

## References

1. F.F. Lange, "Si<sub>3</sub>N<sub>4</sub>-Ce<sub>2</sub>O<sub>3</sub>-SiO<sub>2</sub> Materials: Phase Relations and Strength," Am. Ceram. Soc. Bull., **59** [2] 239-40, 49 (1980).
2. C.L. Quakenbush and J.T. Smith, "Phase Effects in Si<sub>3</sub>N<sub>4</sub> Containing Y<sub>2</sub>O<sub>3</sub> or CeO<sub>2</sub>: II, Oxidation," Am. Ceram. Soc. Bull., **59** [5] 533-37 (1980).
3. G.N. Babini, A. Bellosi, and P. Vincenzini, "Oxidation of Silicon Nitride Hot-Pressed with Ceria," J. Am. Ceram. Soc., **64** [10] 578-84 (1981).
4. D.M. Mieskowski and W.A. Sanders, "Oxidation of Silicon Nitride Sintered with Rare-Earth Oxide Additions," J. Am. Ceram. Soc., **68** [7] C-160-63 (1985).
5. M.K. Cinibulk, G. Thomas, and S.M. Johnson, "RE<sub>2</sub>Si<sub>2</sub>O<sub>7</sub>-Si<sub>3</sub>N<sub>4</sub> Ceramics: I, Design, Fabrication, and Secondary-Phase Crystallization," J. Am. Ceram. Soc., this issue, (1992).
6. F.F. Lange, S.C. Singhal, and R.C. Kuznicki, "Phase Relations and Stability Studies in the Si<sub>3</sub>N<sub>4</sub>-SiO<sub>2</sub>-Y<sub>2</sub>O<sub>3</sub> Pseudoternary System," J. Am. Ceram. Soc., **60** [5-6] 249-52 (1977).
7. J. Ito and H. Johnson, "Synthesis and Study of Yttrialite," Am. Mineralogist, **53** 1940-52 (1968).

8. J. Felsche, "Polymorphism and Crystal Data of the Rare-Earth Disilicates of the Type  $RE_2Si_2O_7$ ," *J. Less-Common Metals*, **21** 1-14 (1970).
9. R.R. Wills, R.W. Stewart, J.A. Cunningham, and J.M. Wimmer, "The Silicon Lanthanide Oxynitrides," *J. Mater. Sci.*, **11** 749-59 (1976).
10. S.C. Singhal, "Thermodynamics and Kinetics of Oxidation of Hot-Pressed Silicon Nitride," *J. Mater. Sci.*, **11** 500-09 (1976).
11. G.N. Babini, A. Bellosi, and P. Vincenzini, "Factors Influencing Structural Evolution in the Oxide of Hot-Pressed  $Si_3N_4$ - $Y_2O_3$ - $SiO_2$  Materials," *J. Mater. Sci.*, **19** 3487-97 (1984).
12. D. Cubicciotti, K.H. Lau, and R.L. Jones, "Rate-Controlling Process in the Oxidation of Hot-Pressed Silicon Nitride," *J. Electrochem. Soc.*, **124** [12] 1955-56 (1977).
13. D. Cubicciotti and K.H. Lau, "Kinetics of Oxidation of Hot-Pressed Silicon Nitride Containing Magnesia," *J. Am. Ceram. Soc.*, **61** [11-12] 512-17 (1978).
14. R.A.L. Drew, S. Hampshire, and K.H. Jack, "Nitrogen Glasses," *Proc. Br. Ceram. Soc.*, **31** 119-32 (1981).
15. F.A. Cotton and G. Wilkinson, Advanced Inorganic Chemistry, 5th Edition, Wiley-Interscience, New York, 1988.

16. J. Felsche and W. Hersiger, "Polymorphs of the Rare-Earth Pyrosilicates  $RE_2Si_2O_7$ - [RE: La, Ce, Pr, Nd, Sm]," *J. Less-Common Metals*, **18** [2] 131-37 (1969).
17. W.D. Kingery, H.K. Bowen, and U.R. Uhlmann, Introduction to Ceramics, 2nd Edition, Wiley-Interscience, New York, 1976.
18. A.J. Pyzik and D.R. Beamon, "Processing, Microstructure, and Properties of Self-Reinforced Silicon Nitride," presented at 92nd Ann. Meeting Am. Ceram. Soc., Dallas, TX, April 22-26, 1990.

**Table 1. Oxidation Kinetics**

Material	Rate Constant (mg <sup>2</sup> /cm <sup>4</sup> hr)	Total Specific Wt. Gain (mg/cm <sup>2</sup> )
Sm <sub>2</sub> Si <sub>2</sub> O <sub>7</sub> -Si <sub>3</sub> N <sub>4</sub>	14.0 x 10 <sup>-4</sup> *	0.644
Gd <sub>2</sub> Si <sub>2</sub> O <sub>7</sub> -Si <sub>3</sub> N <sub>4</sub>	6.1 x 10 <sup>-4</sup>	0.346
Y <sub>2</sub> Si <sub>2</sub> O <sub>7</sub> -Si <sub>3</sub> N <sub>4</sub>	5.1 x 10 <sup>-4</sup>	0.313
Dy <sub>2</sub> Si <sub>2</sub> O <sub>7</sub> -Si <sub>3</sub> N <sub>4</sub>	5.0 x 10 <sup>-4</sup>	0.314
Yb <sub>2</sub> Si <sub>2</sub> O <sub>7</sub> -Si <sub>3</sub> N <sub>4</sub>	3.7 x 10 <sup>-4</sup>	0.268
Er <sub>2</sub> Si <sub>2</sub> O <sub>7</sub> -Si <sub>3</sub> N <sub>4</sub>	3.3 x 10 <sup>-4</sup>	0.252

\* Determined for the period 72-192 hr (parabolic behavior)

**Table 2. X-ray Diffraction of Oxidized Surfaces**

Material	Major Phases	Minor Phases
Y <sub>2</sub> Si <sub>2</sub> O <sub>7</sub> -Si <sub>3</sub> N <sub>4</sub>	β-Y <sub>2</sub> Si <sub>2</sub> O <sub>7</sub> , SiO <sub>2</sub> *	Si <sub>2</sub> ON <sub>2</sub> , β-Si <sub>3</sub> N <sub>4</sub>
Sm <sub>2</sub> Si <sub>2</sub> O <sub>7</sub> -Si <sub>3</sub> N <sub>4</sub>	A-Sm <sub>2</sub> Si <sub>2</sub> O <sub>7</sub> , SiO <sub>2</sub>	Si <sub>2</sub> ON <sub>2</sub> , β-Si <sub>3</sub> N <sub>4</sub>
Gd <sub>2</sub> Si <sub>2</sub> O <sub>7</sub> -Si <sub>3</sub> N <sub>4</sub>	δ-Gd <sub>2</sub> Si <sub>2</sub> O <sub>7</sub> , SiO <sub>2</sub>	Si <sub>2</sub> ON <sub>2</sub> , β-Si <sub>3</sub> N <sub>4</sub>
Dy <sub>2</sub> Si <sub>2</sub> O <sub>7</sub> -Si <sub>3</sub> N <sub>4</sub>	δ-Dy <sub>2</sub> Si <sub>2</sub> O <sub>7</sub> , SiO <sub>2</sub>	α-Dy <sub>2</sub> Si <sub>2</sub> O <sub>7</sub> , Si <sub>2</sub> ON <sub>2</sub> , β-Si <sub>3</sub> N <sub>4</sub>
Er <sub>2</sub> Si <sub>2</sub> O <sub>7</sub> -Si <sub>3</sub> N <sub>4</sub>	β-Er <sub>2</sub> Si <sub>2</sub> O <sub>7</sub> , SiO <sub>2</sub>	Si <sub>2</sub> ON <sub>2</sub> , β-Si <sub>3</sub> N <sub>4</sub>
Yb <sub>2</sub> Si <sub>2</sub> O <sub>7</sub> -Si <sub>3</sub> N <sub>4</sub>	β-Yb <sub>2</sub> Si <sub>2</sub> O <sub>7</sub> , SiO <sub>2</sub>	Si <sub>2</sub> ON <sub>2</sub> , β-Si <sub>3</sub> N <sub>4</sub>

\* as α-cristobalite

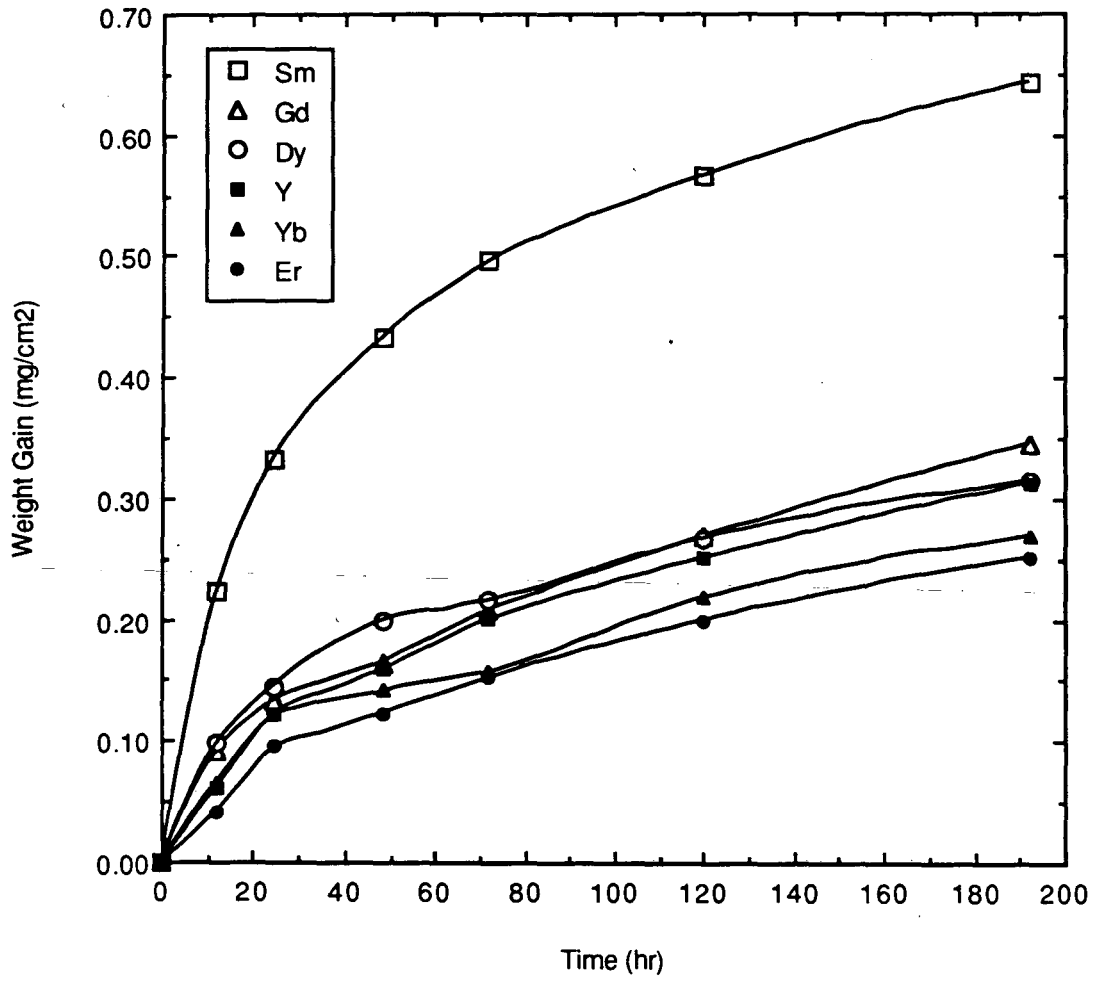
## Figure Captions

Figure 1. Plot of specific weight gain as a function of time, at 1400°C.

Figure 2. Parabolic plot of specific weight gain as a function of time, at 1400°C.

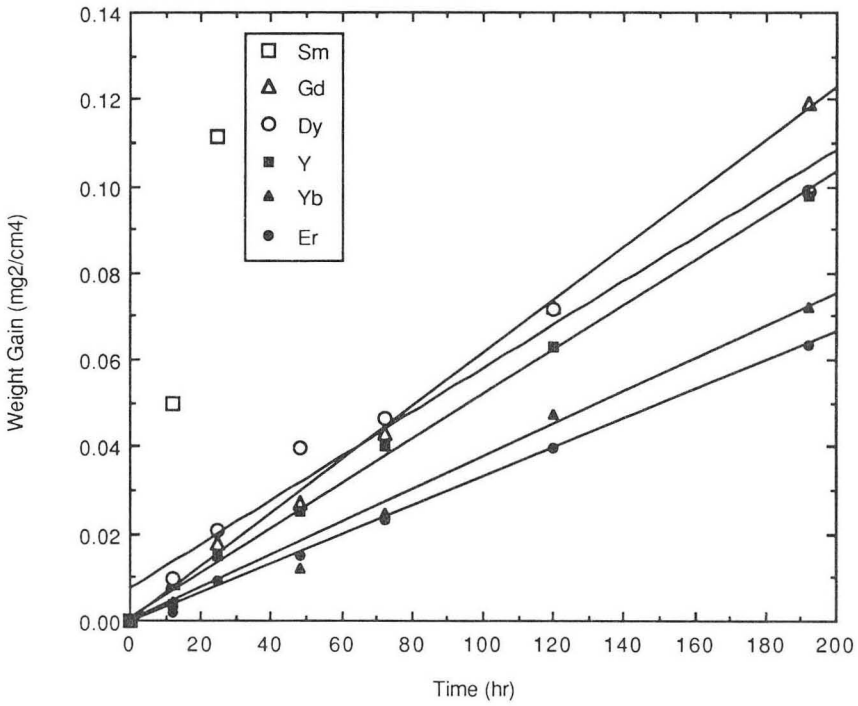
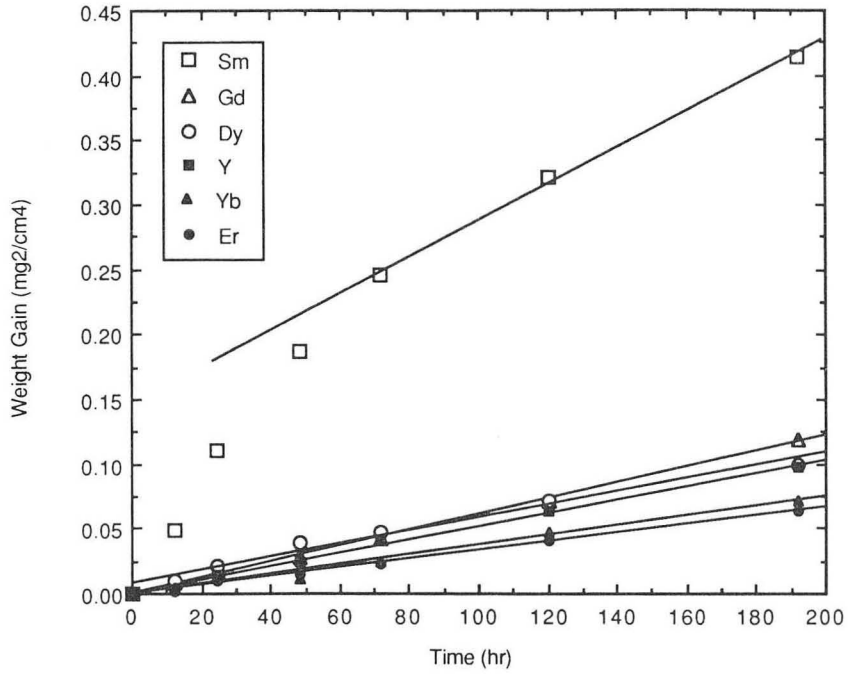
Figure 3. Scanning electron micrographs of the oxidized surfaces imaged using secondary electrons, showing surface topography and morphology and preference in direction of disilicate growth.

Figure 4. Scanning electron micrographs of the oxidized surfaces imaged using backscattered electrons to obtain compositional contrast. Darkest-contrast phase is cristobalite, medium-contrast phase is residual silicate, and brightest-contrast phase is the rare-earth disilicate.



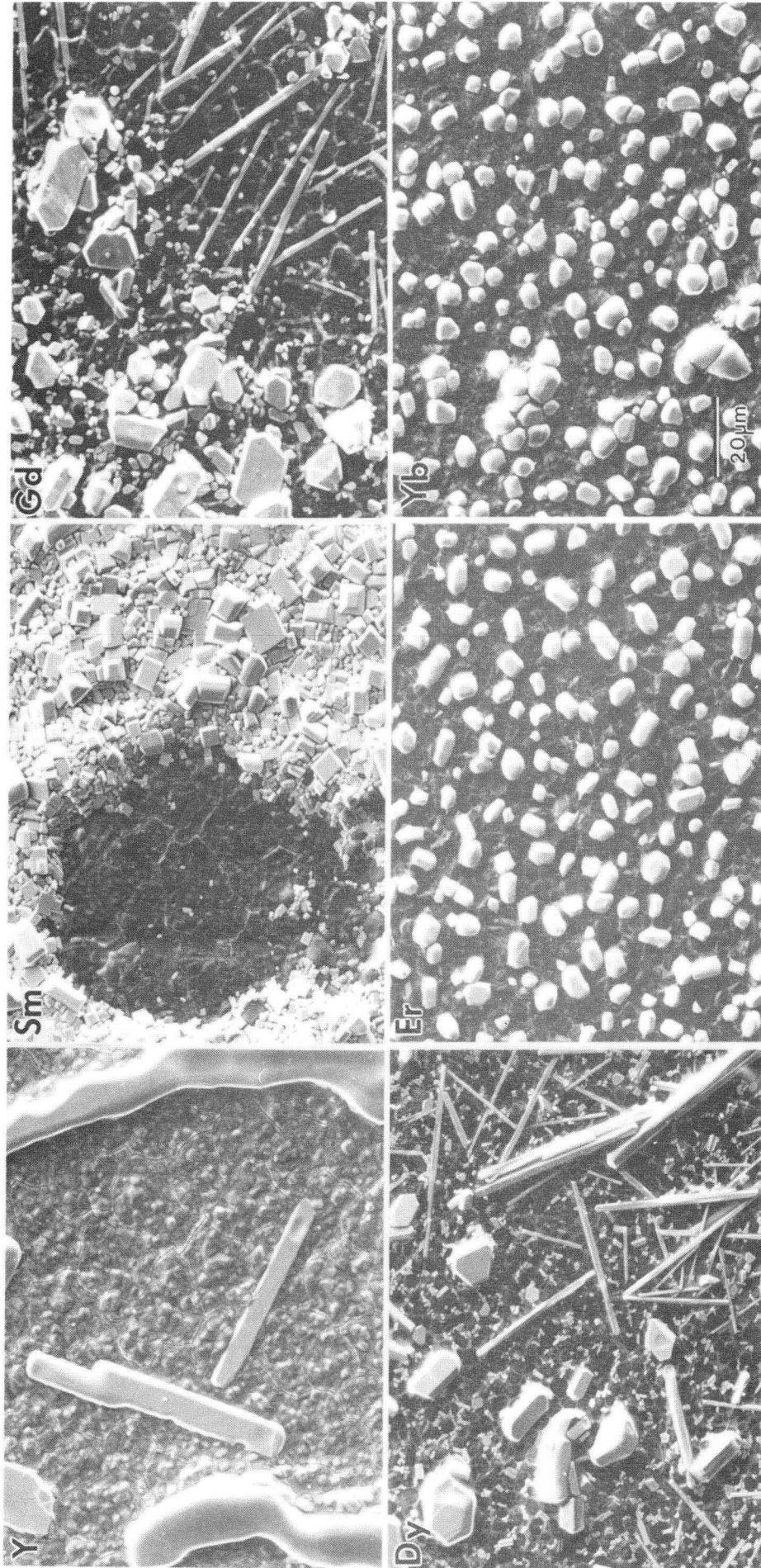
XBL 916-1287

Figure 1



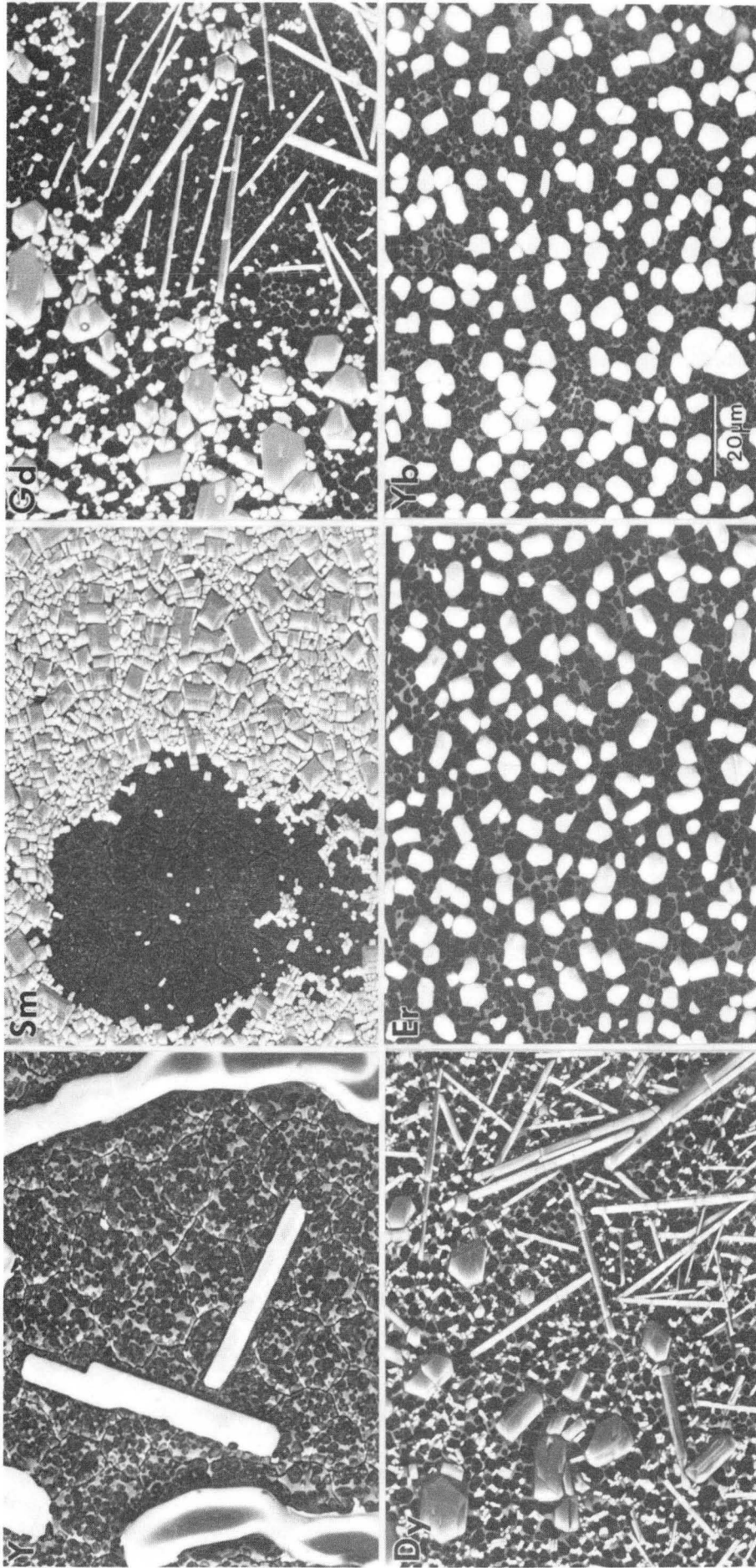
XBL 917-1608

Figure 2



XBB 913-1898

Figure 3



XBB 913-1897

Figure 4

LAWRENCE BERKELEY LABORATORY  
UNIVERSITY OF CALIFORNIA  
INFORMATION RESOURCES DEPARTMENT  
BERKELEY, CALIFORNIA 94720